Acta Geologica Sinica (English Edition), 2023, 97(1): 55–67

Intra-continental Orogeny: Insights from Magnetotelluric Data into the Mesozoic Uplift History of the Eastern Jiangnan Orogen in South China

ZHANG Kun[1, 2], LÜ Qingtian[1, 2, *], ZHAO Jinhua[1, 2], YAN Jiayong[1, 2], LUO Fan[3], MAN Zuhui[1, 2, 4], XIAO Xiao[5], ZHANG Gang[6] and YONG Fan[7]

[1] *Chinese Academy of Geological Sciences, Beijing 100037, China*
[2] *Key Laboratory of Deep Earth Science and Exploration Technology of Ministry of Natural Resources*
[3] *East China Institute of Technology, Nanchang 330013, China*
[4] *China University of Geosciences (Wuhan), Wuhan 430074, China*
[5] *Central South University, Changsha 410083, China*
[6] *China University of Geosciences (Beijing), Beijing 100086, China*
[7] *Institute of Geophysical and Geochemical Exploration, Chinese Academy of Geological Sciences, Langfang, Hebei 065000, China*

Abstract: Despite extensive efforts to understand the tectonic evolution of the Jiangnan Orogen in South China, the orogenic process and its mechanism remain a matter of dispute. Previous geodynamic studies have mostly focused on collisional orogeny, which is commonly invoked to explain the Jiangnan Orogen. However, it is difficult for such hypotheses to reconcile all the geological and geophysical data, especially the absence of ultrahigh-pressure metamorphic rocks. Based on the magnetotelluric data, we present a group of resistivity models produced through the combination of two-dimensional and three-dimensional inversions, revealing the geo-electrical structures of Jiangnan and a typical collisional orogen. In our models, the resistive crust is separated into three parts by a prominent conductive layer with opposite dipping directions on both sides. A special thrust-nappe system, which is different from that developed in a typical collisional process, is revealed in the Jiangnan Orogen. This structure suggests a process different from the simple collisional orogeny. To interpret our observations, an 'intra-continental orogeny' is proposed to address the development of the Jiangnan Orogen in the Mesozoic. Furthermore, this 'reworked' process may contain at least two stages caused by the decoupling of the lithosphere, which is revealed by an extra conductive layer beneath Jiangnan.

Key words: magnetotelluric sounding, 2D inversion, 3D inversion, intra-continental orogeny, Jiangnan Orogen

Citation: Zhang et al., 2023. Intra-continental Orogeny: Insights from Magnetotelluric Data into the Mesozoic Uplift History of the Eastern Jiangnan Orogen in South China. Acta Geologica Sinica (English Edition), 97(1): 55–67. DOI: 10.1111/1755-6724.14950

1 Introduction

The Jiangnan Orogen (JNO) is the Proterozoic collision suture between the Yangtze and Cathaysia blocks (Chen et al., 1991; Shu et al., 2020), which are the two major sub-blocks of the South China craton (Wang et al., 2017). Huang (1954) first proposed the concept of 'Jiangnan paleo-block' for the Jiangnan area. With further geological studies, this region has variously been described as the 'Jiangnan Block' (Huang, 1954), 'Jiangnan Geo-anticline' (Huang, 1959), 'Jiangnan Geo-axis' (Huang, 1960), 'Jiangnan Ancient Arc' (Guo et al., 1977) and the 'Suture zone of Hunan, Jiangxi and Zhejiang provinces' (Xu et al., 1987). After decades of research on the ophiolite and magmatic rocks, it was widely accepted that a Meso-Neoproterozoic orogenic belt existed in the southeast margin of the Yangtze (e.g., Shu et al., 1995; Zhou et al., 2009). The concept of the 'Jiangnan Orogen' (Shu et al., 1995, 2020) was then proposed and accepted by the research community.

The formation and evolution of the JNO is believed to be key to understanding the regional evolution and geological questions of South China, including the orogeny and related magmatism (Shu et al., 2020). Previous models for the formation of the JNO were mostly focused on collisional processes between Yangtze and Cathaysia, attributing the orogeny to a continental collision. Hsü et al. (1988) suggested the JNO was formed by the collision between Yangtze and Cathaysia in the Indosinian (~257–205 Ma), while Xu et al. (1992) proposed a collision in the early Paleozoic. However, the lack of oceanic crust residuum does not support a collision after the Paleozoic (Shu et al., 2011). Later, Wong et al. (2011) suggested that the Yangtze and Cathaysia blocks might not be completely amalgamated in the Neoproterozoic. But the similar signatures of the Cambrian–Silurian sandstone samples in both Yangtze and Cathaysia indicated that the two blocks had been collaged prior to the Paleozoic (Wang et al., 2010). Moreover, the absence of ultrahigh-pressure metamorphic

* Corresponding author. E-mail: lqt@cags.ac.cn

rocks, which is the typical feature of a collisional orogeny, leads to ambiguity in the explanations of the formation mechanism of the JNO. Zhao et al. (2015) hence proposed a 'divergent double subduction' model as a compromise for a collisional orogeny without ultrahigh-pressure metamorphism. Afterwards, Zhang and Dong (2019) proposed that the subduction-collision accretion and intra-continental orogen could be a causal cycle in the late Mesozoic (170–135 Ma), forming the JNO. All of these contradictions suggest that the orogeny in question is far more complex than previously predicted and may not be explained by a simple system in its geological history.

Multiple tectonic events have developed in the JNO during the Neoproterozoic, early Paleozoic and Mesozoic (containing the Indosinian and Yanshanian), resulting in extremely complex geological structures. Furthermore, the orogenic process of the JNO is closely related to the tectonic events in its adjacent areas, such as the subduction -collision process between the North China Block and the Yangtze, in which the Lower Yangtze Depression (LYD) to the west of the JNO is believed to be the suture (Chang et al., 1991, 1996). Hence, deep constraints of geophysics of the crust crucially require to be understood for the deformation of the JNO. Due to the high horizontal resolution and sensitivity for conductive fluids/melts, magnetotelluric analysis has been widely used to understand the tectonic history of the crust (e.g., Dong et al., 2016; Zhang et al., 2019a, b). Considering previous magnetotelluric results and interpretations on the Dabie Orogenic Belt (DOB) and the LYD (Zhang et al., 2019a, 2020), two new magnetotelluric profiles were acquired across the DOB, middle LYD and eastern JNO (Fig. 1). Based on the new geo-electrical models, an intra-continental orogenic event is proposed, leading to further understanding of the evolutionary phases of the JNO in the Mesozoic.

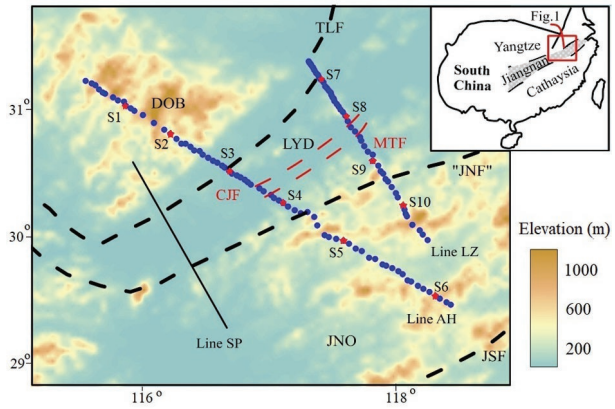

Fig. 1. Topographic map of the Lower Yangtze area, superposed with major faults and suture zones.
The magnetotelluric stations used in the inversion and interpretation are shown in blue circles. Previously proposed tectonic boundaries are shown as black dashes. Previous magnetotelluric profile is shown as black line. Yangtze fault: Yangtze River fault; main thrust fault: main thrust fault (Lü et al., 2015). DOB: Dabie Orogenic Belt; LYD: Lower Yangtze Depression; JNO: Jiangnan Orogen. Geological boundary contains Tancheng–Lujiang fault (TLF) on the east of the DOB (Lü et al., 2021), 'Jiangnan fault' (JNF) (Jiang et al., 2013) on the east of the LYD and the Jiangshan-Shaoxing fault (JSF) (Wang et al., 2017) on the east of the JNO. Stars (S1–S10) are the location of the curves shown in Figure 2.

2 Geological Setting

The Yangtze Block has metamorphic crystallization basement formed in the Archean (Ge et al., 2013) and widespread Phanerozoic supracrustal sediments preserved (Zhai and Zhou, 2015). The eastern Yangtze comprises two types of basements, namely the metamorphic basement beneath the LYD and the fold basement beneath the JNO (Chang et al., 1996; Dong et al., 2011). The cover strata contain sediments from the Sinian to Quaternary, missing the Middle–Lower Devonian strata. Granitoid intrusions and subvolcanic complexes are also present in the Yangtze (Chang et al., 1991). The LYD is located on of the northeast part of the Yangtze, suggested to be bordered by the Tancheng–Lujiang fault to the northwest (Zhao et al., 2016) and the Jiangnan fault to the southeast (Lü et al., 2021) (Fig. 1). To the east of the LYD, the JNO is located on the southeast part of the Yangtze.

The JNO is suggested to be the result of a collision between the Yangtze and the Cathaysia blocks during the late Neoproterozoic (870–820 Ma), with a series of tectonic events recorded (e.g., Charvet et al., 1996; Wang et al., 2004; Shu et al., 2020). The Neoproterozoic strata are exposed in the JNO, which contain two metamorphic sequences lacking ultrahigh-pressure metamorphic rocks (Pirajno, 2013). On the contrary, an ultrahigh-pressure metamorphic belt (DOB; Ni et al., 2013) has been formed to the west of the JNO, due to the collision between the Yangtze and North China (Zhao et al., 2016).

The strata in the study area have an age distribution pattern of old-new-old from west to east (Wang et al., 2012) on the surface. This means the Precambrian basement is exposed in the DOB and JNO, with the Paleozoic–Cenozoic sedimentary strata exposed in the LYD. A series of upper crustal fold-thrust-nappe structures have formed under a compressional stress, which is believed to be interrelated with the subduction-collision process between the DOB and the Yangtze (Faure et al., 2001). Moreover, a double-sided thrust-nappe structure (NW dipping in the west, SE dipping in the east) is believed to have developed, with the Yangtze fault and the main thrust fault as its center (Lü et al., 2015; Zhang et al., 2019a). After the compressional evolution, numerous geochemical and geochronological studies on adakitic rocks and A-type granites in the LYD (e.g., Zhou et al., 2016; Shu et al., 2020 and references therein) indicate a conversion to an extensional regime (Ren et al., 1997) in the late Mesozoic.

3 Data Processing and Analysis

3.1 Data processing

Data from 119 broadband MT stations were acquired, using commercial instruments (MTU-5A produced by the Phoenix Co., Ltd., Canada) along two new profile lines (AH and LZ) in the middle section of the eastern Yangtze and its adjacent areas, with site spacing of 2–5 km. Time series were measured for two perpendicular electric channels (Ex and Ey, where x denotes the north–south direction and y denotes the east–west direction) and three magnetic channels (Hx, Hy, and Hz, where Hz is the

vertical component). Time series were transformed into frequency data by fast Fourier transform, then robust estimation technology with remote reference techniques was used to calculate the MT transform function, which is also called impedance tensor (Z) and is used to calculate the apparent resistivity ($\rho = |Z|^2/\omega\mu$) and impedance phase (P = atan[Zima/Zreal]). The commercial program banded with MTU-5A was used to carry out the above pre-processing. Roughly smooth data curves were obtained over a period range of 0.003–1000 s. The corresponding skin depths suggest a penetration of greater than 150 km, as calculated by the Niblett–Bostick transformation method (Jones et al., 1983) in which average apparent resistivity is larger than 100 Ω·m.

In addition, a de-noising (Zhang et al., 2019a) technology was used to automatically mask the noise-influenced data, based on 1D inversion. Data (apparent resistivity and impedance phase) with a large misfit was deleted after a series of 1D inversions, in order to get a better input datum for the following 2D and 3D inversions. This repeated process stopped when the misfit of all the remaining data could be accepted. Ten results of data de-noising for strong noise influence are shown in Fig. 2. Another manual selection process was carried out to confirm the quality of the data and avoid false selection from the de-noising process.

3.2 Phase tensor analysis

The phase tensor (Caldwell et al., 2004) was applied in this study to analyze dimensionality and strike of the MT data, using a software platform named EMinv (provided by Zhang Kun). It can be shown as an ellipse for each period of data, using three values: Φ_{max} (the maximum phase), Φ_{min} (the minimum phase) and β (the skew angle). fmax and fmin corresponded to the major and minor (polarization) axes of the ellipse, representing the two orthogonal electrical principal axes that indicate the possible strike directions. For 1D condition, the ellipse is a circle. The skew angle (β) is an indicator of the anisotropy in the MT data, which represents dimensionality of the electrical material.

The ellipses (Fig. 3) show weak polarization and a generally low skew angle in the high-frequency range (< 0.1 s, the penetration depth is ~0–3 km). However, the ellipses abruptly rotate to a dominant NW direction with a relatively high skew angle in the mid-frequency range (period range 0.01–10 s, penetration depth is ~1–15 km) at 15 and 115 km along profile LZ, as well as 100 and 200 km along profile AH, indicating highly asymmetric conductive structures. These variations reflect the positions of the fault and the boundaries between the DOB (North China), LYD and the JNO. In the long period range (>10 s, penetration depth is >15 km), the extremely flattened ellipses (strong polarization) with directional variations suggest the existence of abrupt lateral geo-electrical interfaces in the middle-lower crust of the LYD and the JNO. Moreover, dark colors of the skew angle reflect 3D structures. Therefore, an extra 3D inversion after 2D inversion was applied to reconcile the linear distribution of the stations and the 3D structures in the study area (see Section 4).

3.3 Pseudo-sections of the apparent resistivity and impedance phase

Data were rotated to the profile direction for analysis and inversion (y is rotated parallel to the line direction and x is perpendicular). Pseudo-sections are used to display our MT data, which are shown in a frequency range of 100 –0.01 Hz to spotlight the major crustal structures). Our study area can be divided into three major parts (Figs. 4–5), including two resistive zones on both sides and a relatively conductive zone in the middle. Their boundaries are located at 10 and 120 km along line LZ, as well as 100 and 190 km along line AH. Moreover, the electrical characteristics of each part are different accross the two lines. In part I (Figs. 4–5), a resistor roughly exists

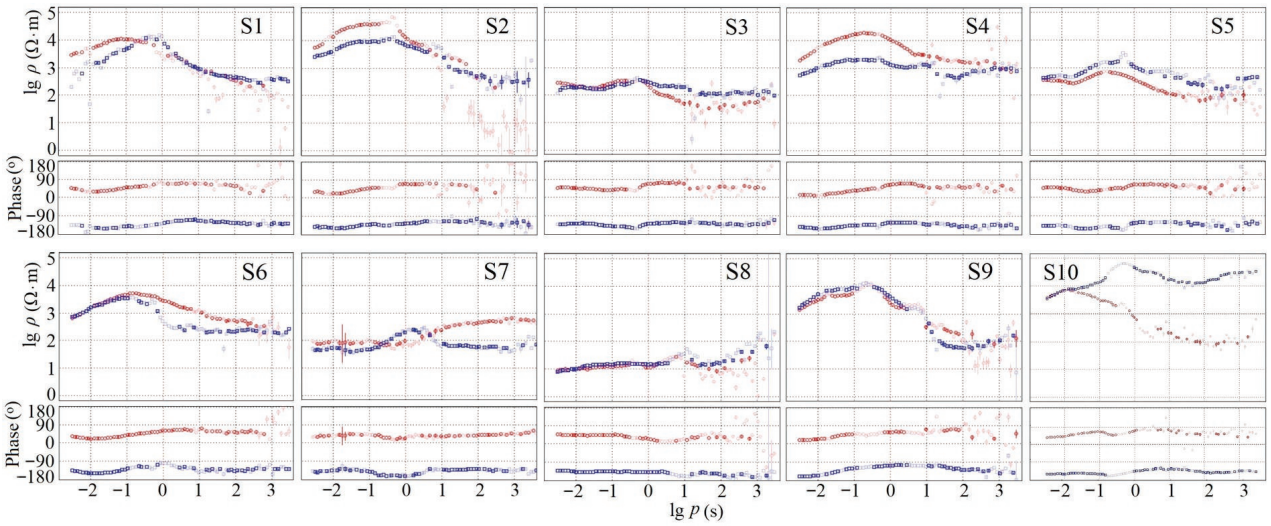

Fig. 2. Typical results of data processing and de-noising of partial stations, whose locations are shown in Figure 1.
Red squares are XY component of apparent resistivity and impedance; blue squares are YX component of apparent resistivity and impedance. Translucent squares are original data before de-noising.

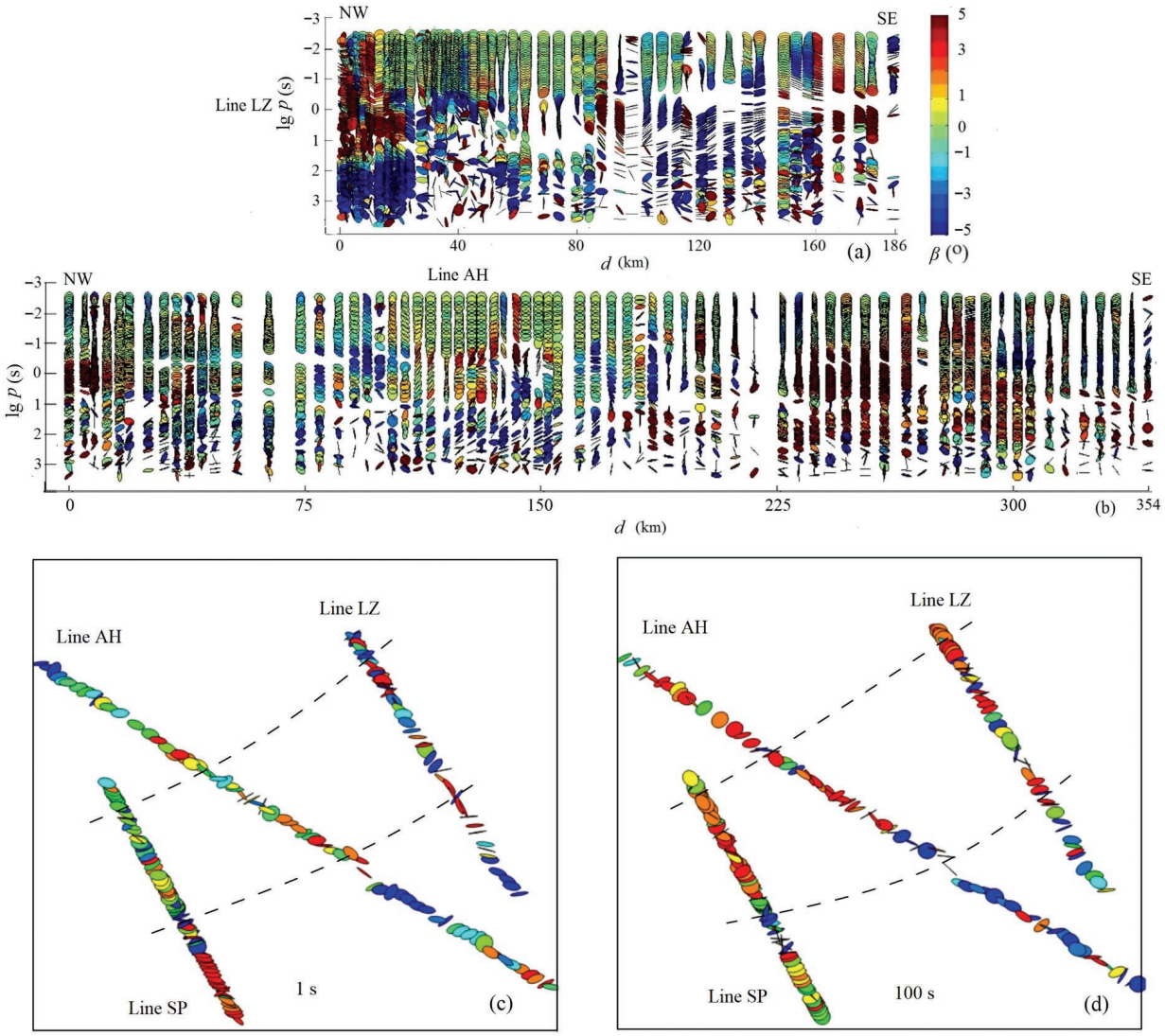

Fig. 3. Phase tensor results of all the sites on line LZ (a) and line ZH (b) and results of frequency slices (c–d) of all the three profiles (including line SP).

throughout the entire period range on profile LZ, but two layers with different resistivity are observed on profile AH. This indicates an internal variation in the structures from south to north. In part II, a conductor exists throughout the entire frequency range on profile LZ, but more details are revealed on profile AH. In part III, a resistor roughly exists throughout most of the period range in both profiles, but the injection of the conductors is stronger on profile AH. The impedance phase has electrical characteristics like those of the apparent resistivity. Moreover, we found a large phase of YX data at the boundary of parts II and III, increasing from 90° to 180°. This may indicate a 'L-shaped' conductor (Ichihara and Mogi, 2009) in the deep crust.

4 Inversions and Interpretation

4.1 Inversions

The non-linear conjugate gradients (NLCG) method (Rodi and Mackie, 2001; Zhang et al., 2014a, b, 2017) was used to invert our MT data. Based on the dimensional analysis, a combination of 2D and 3D inversion (Zhang et al., 2019a) has been used to compromise the multiplicity induced by linearly distributed stations in a 3D mesh, as the data show a complex deep structure with three dimensions. However, data were measured on profiles without lateral controls between the profiles, focusing on the major tectonics directed NE–SW. Moreover, previous studies (Zhang et al., 2019a) showed a successful application of the combination of 2D and 3D inversion, using 2D models as the constraints. Therefore, the 3D inversion here was individual for each profile, using the 2D inversion result as the initial model. In the two 3D coordinate systems, the X axis was rotated perpendicular to profile LZ and AH (the Y axis is parallel to the profile), respectively.

First, the 2D inversion of the apparent resistivity and

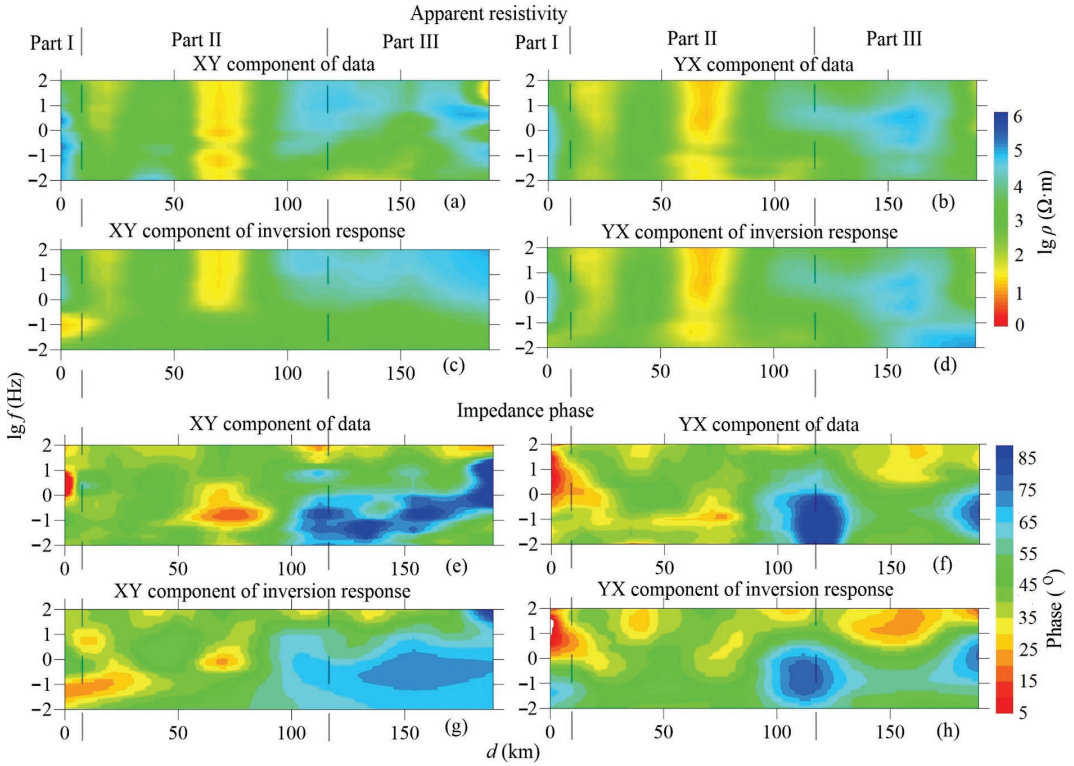

Fig. 4. The apparent resistivity and impedance phase comparison of measured data and inversion responses for line LZ.
(a) XY component of apparent resistivity of data; (b) YX component of apparent resistivity of data; (c) XY component of apparent resistivity of inversion response; (d) YX component of apparent resistivity of inversion response; (e) XY component of impedance phase of data; (f) YX component of impedance phase of data; (g) XY component of impedance phase of inversion response; (h) YX component of impedance phase of inversion response.

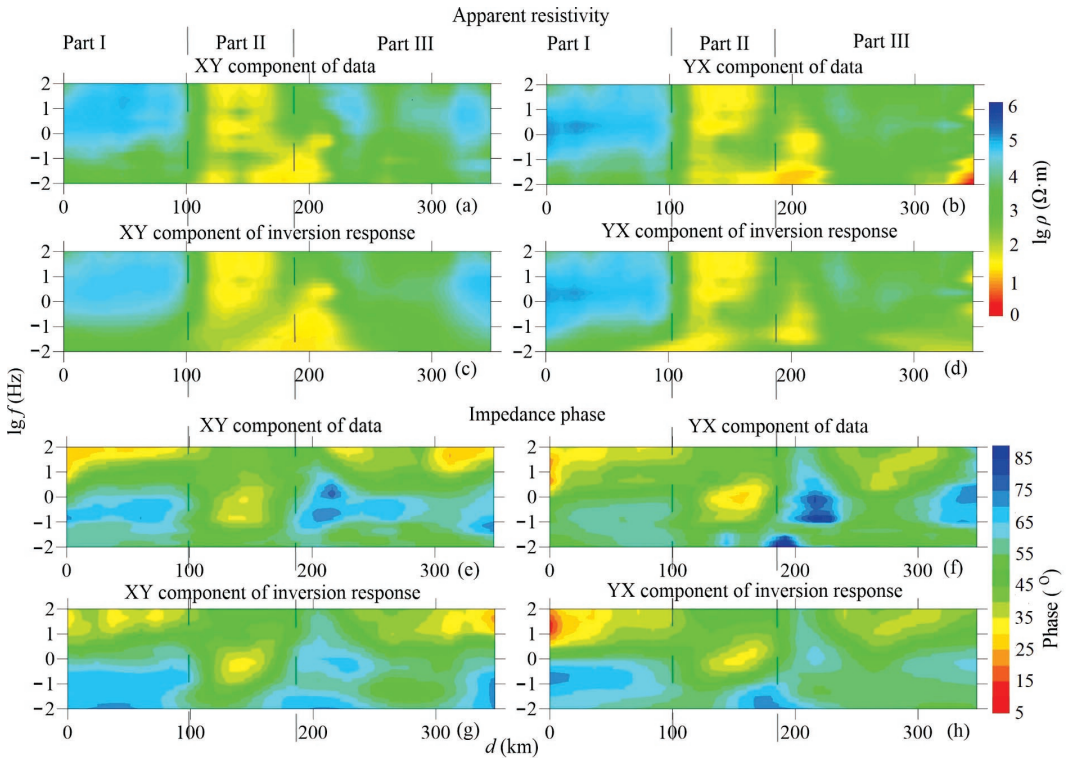

Fig. 5. The apparent resistivity and impedance phase comparison of measured data and inversion responses for line AH.
(a) XY component of apparent resistivity of data; (b) YX component of apparent resistivity of data; (c) XY component of apparent resistivity of inversion response; (d) YX component of apparent resistivity of inversion response; (e) XY component of impedance phase of data; (f) YX component of impedance phase of data; (g) XY component of impedance phase of inversion response; (h) YX component of impedance phase of inversion response.

impedance phase was carried out using the program from Zhang Kun (Zhang et al., 2011), namely EMinv. The data error was 10% for apparent resistivity and 10° for phase, because the phase data were not as good as the apparent resistivity and the large phase increased the RMS of the 2D inversion. The model domain had dimensions of 1200 km (Y) × 900 km (Z) for profile LZ and 3400 km (Y) × 900 km (Z) for profile AH. Nominal grid-spacing in the central part of the domain was approximately 1–2 km. The initial model was a half-space (100 Ω·m) constrained by the bathymetry.

The 3D inversion for the data of the full impedance tensor was then carried out using EMinv, based on an improved NLCG algorithm (Zhang et al., 2013, 2017) after Newman and Alumbaugh (2000). The data error floor was set as an absolute value (Zreal × 0.05 + Zimag × 0.05). The model domain was 100 km (X) × 1200 km (Y) × 900 km (Z) for profile LZ and 100 km (X) × 3400 km (Y) × 900 km (Z) for profile AH. The nominal grid-spacing in the central part was 1.5 km. The initial model of 3D inversion (including bathymetry) was the 2D inversion result of each profile with the same value for the X-direction extension.

For the two inversion processes, data in the range 0.003–1000 s were used after selection (containing automatic de-noising and manual selection). In addition, the zero-cost static shift correction method was used, which treated the apparent resistivity and impedance phase as prior information for the static shift justification and used inversion as the correction instrument by constraining the initial model (Zhang et al., 2016). After parameter tests, the regularization factor was set to a value of 3 to balance the normalized misfit and model roughness (Fig. 6) in 3D inversion. The lower overall misfit and increasing model roughness of the 3D inversions indicate that the geo-electrical models are better updated by the releasing of off-profile structures. Moreover, the comparison of the data and inversion responses (apparent resistivity and impedance phase) of the preferred models (Figs. 4–5) exhibits good consistency in most areas and periods.

4.2 Boundaries and distinct structures of the DOB, LYD and JNO

MT data generally provide a better resolved estimate of the conductance of a particular layer rather than its actual resistivity (Jones, 1992). In combination with the resistivity models (Fig. 7), the depth-integrated conductance, which can be estimated by calculating the $S = h/\rho$ of each layer over a given depth range, is further used to distinguish the tectonic boundary and broad conductors. Introducing the previous inversion result of line SP, resistivity models, for which the depth of investigation (> 40 km) of all the stations is much larger than the target, were used to calculate the distinct conductance over 0–40 km and 30–40 km of the three profiles (Fig. 8).

Previous seismic research indicates the thickness of sedimentary cover in the upper crust in our study area is ~ 10 km, whilst the thickness of the Precambrian basement in the mid-lower crust is 10–20 km (Lü et al., 2015). These seismic results of crustal stratification are used here to explain the depth range of the anomalies. Bounded by horizontal interfaces (S2-S3, Fig. 7) and distribution of high conductance (Fig. 8), a major conductor (C2) is

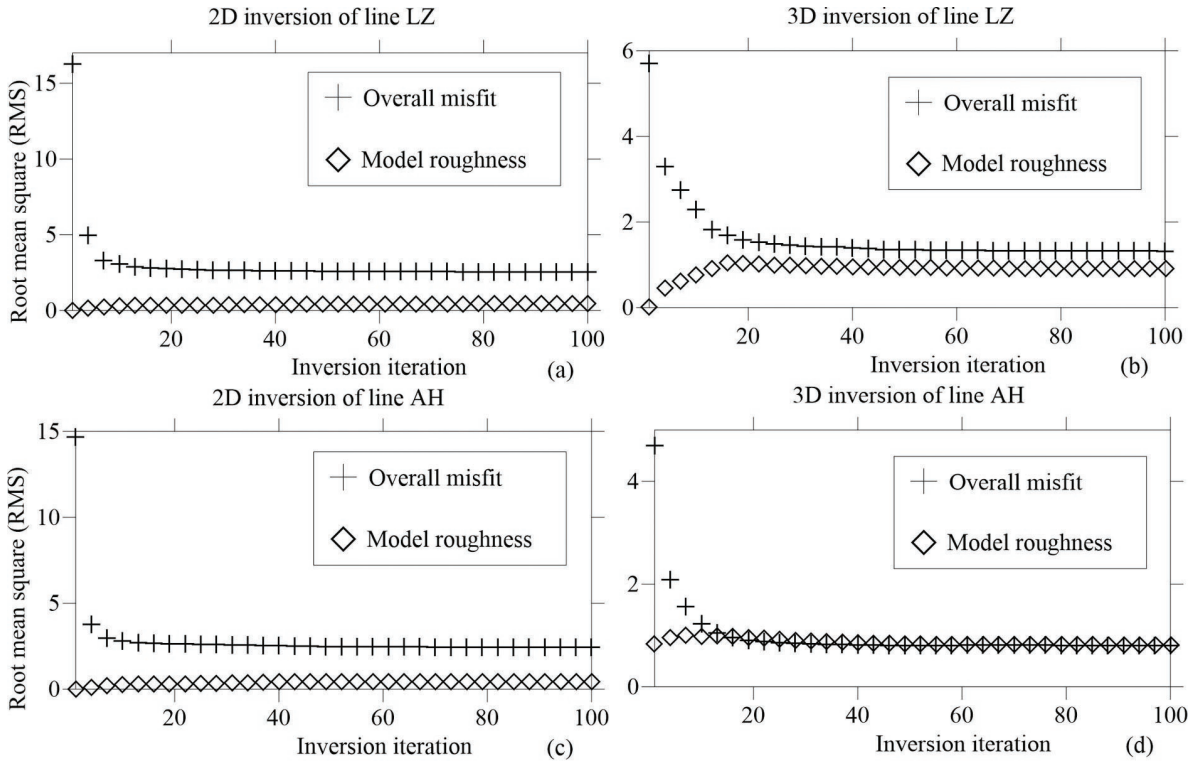

Fig. 6. Data misfit and model modification of line LZ (a–b) and AH (c–d).

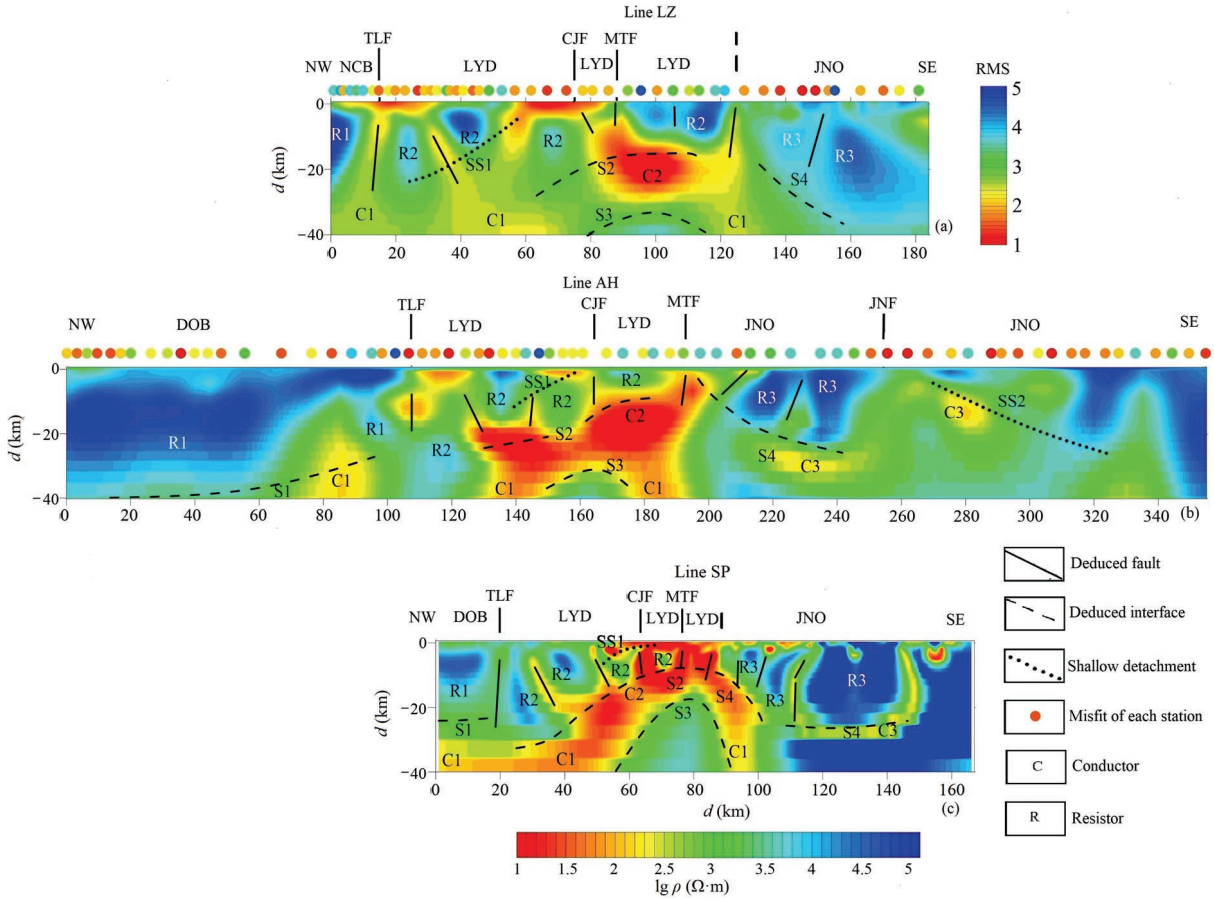

Fig. 7. Vertical sections of the geo-electrical model for line LZ (a), line AH (b) and line SP (c).
The model resistivity and data misfit share the same color bar. Interpretation of line SP is based on the previous results (after Zhang et al., 2019a). The distribution of the Yangtze fault (CJF) and the main thrust fault (MTF) are from, or deduced by, the deep seismic results from Lü et al., 2014. TLF: Tancheng–Lujiang fault; JNF: Jiangnan fault; DOB: Dabie Orogenic Belt; LYD: Lower Yangtze Depression; JNO: Jiangnan Orogen.

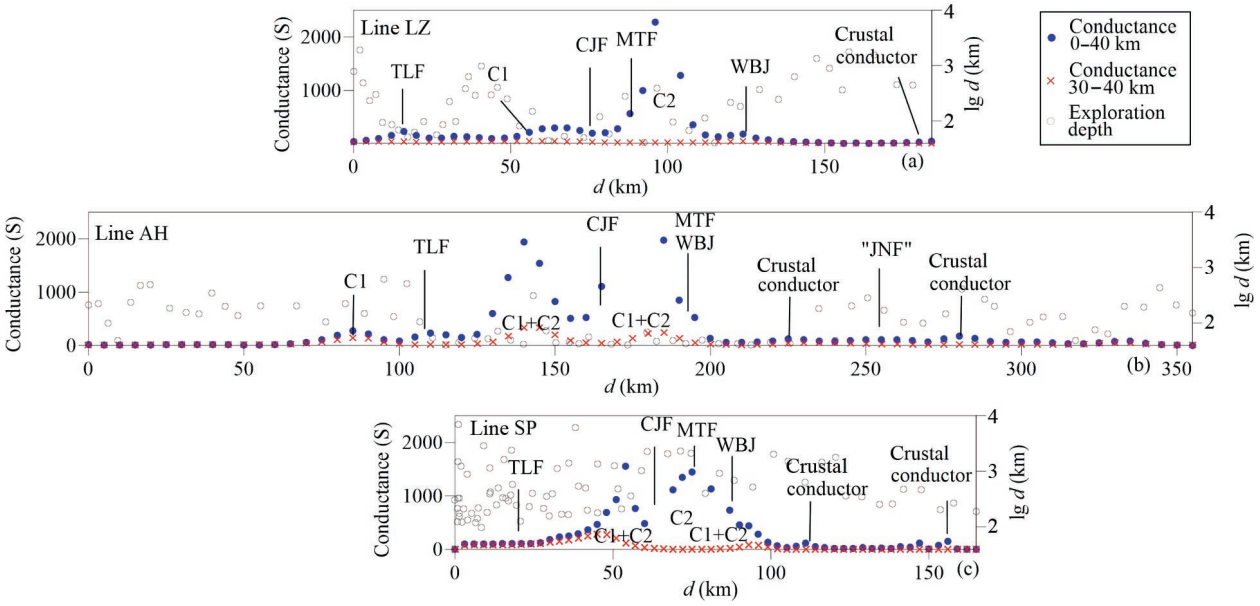

Fig. 8. Depth-integrated conductance map calculated for crust (0–40 km) and Moho (30–40 km) of line LZ (a), line AH (b) and line SP (c).
CJF: Yangtze fault; MTF: main thrust fault; TLF: Tancheng–Lujiang fault; JNF: Jiangnan Fault; DOB: Dabie Orogenic Belt; LYD: Lower Yangtze Depression; JNO: Jiangnan Orogen; WBJ: western boundary of Jiangnan.

revealed in the mid-to-lower crust of the LYD and partially connects with a conductor (C1) in the lower crust. The LYD is the subduction-collision suture between North China and the Yangtze (Li et al., 2015). It is believed to have desorbed massive amounts of water during the dehydration process of the subduction slab (Zheng et al., 2016), which could have led to the partial melting. In addition, melting-assimilation-storage-homogenization (MASH) processes (Wang et al., 2001; Lü et al., 2013, 2021) have probably occurred following this regional tectonic event (Lü et al., 2015; Zhou et al., 2016), as supported by the study of isotope geochemistry (Zhou et al., 2016). C1 and C2 most likely represent the hydrogen fluids and/or partial melts, while C2 may also represent the detachment layer.

The abrupt truncation of C2 and decreasing conductance on both its sides represent the boundary position of the LYD in the mid-to-lower crust. In the upper-to-middle crust, the structure, composed of the major resistors (R1–R3) with distinct features, shows a symmetrical distribution around the LYD overlying C2. Unlike R1 and R3, R2 presents stronger lateral and vertical variations, so can be used to constrain the range of the DOB and JNO in the upper-to-middle crust. The southward extension of the Tancheng–Lujiang fault is hence revealed to be a crustal boundary between the LYD and DOB (Figs. 7–8). It has a horizontal distribution of ~10–20 km at different depths (Fig. 9a). Moreover, a new electrical interface between the LYD and JNO is revealed as the western boundary of the JNO (WBJ, Fig. 8), which has a horizontal distribution of ~10–25 km at different depths (Fig. 9a).

The DOB is accepted as a typical collisional orogen (e.g., Zhao et al., 2016) where multiple and large-scale magmatism (Li et al., 2015; Lü et al., 2015, 2021) is revealed by the Mesozoic magmatic rocks (Mao et al., 2014). A relatively stable crust beneath the DOB is suggested by a widespread resistor (R1, Fig. 7b) and low conductance (Fig. 8b). In contrast, crustal conductors, which are absent beneath the DOB, are revealed beneath the JNO (Fig. 8). This indicates a different tectonic-magmatic process of the JNO compared to the DOB. A superimposed tectonic process is suggested having developed in the JNO by the C3 (beneath S4) during an extensional event. To test the possibility of the existence of this important conductor (C3), a moderate resistive (3000 Ω·m) belt beneath R3 and S4 was introduced to the model of line AH (Appendix Fig. 1a–b). A second inversion was performed using the modified model as the starting model. As the final misfit of the second inversion is close to the original inversion (1.19 vs 1.18), the modified resistive belt is updated to a major conductor (C3), as revealed in the preferred model. Responses of the second inversion seem to be similar as the original (Supp. Fig. 1c–d), therefore the existence of C3 is reliable.

5 Discussion

5.1 Double thrust nappe system across the Lower Yangtze Depression and Jiangnan Orogen

A large-scale fold-thrust system in the LYD is indicated by the A-type granitic magmatism and pull-apart basin during the Late Mesozoic (Wang et al., 2012), and has furthermore been proposed to be the major component of a double thrust system (Ling et al., 2009; Li et al., 2012; Lü et al., 2015). Specifically, the Yangtze fault and the main thrust fault (Lü et al., 2015, Fig. 1) are two important fault zones by which the thrust-nappe can be divided into two major tectonic systems, namely the LYD nappe and the JNO nappe. This double thrust-nappe system is strongly consistent and is coupled with the upper-middle crustal structures (R2–R3 and adjacent anomalies) revealed in our models. It is represented as a symmetrical arch in general, composed of a series of superposed structures from both sides to the center. C2 and R2–R3 are inferred as the major detachment and superposed strata, respectively, while the shallower conductive belts connected with C2 are the thrusts (Fig. 7).

Beneath the LYD, a left-facing ‘crocodile’ structure (Lü et al., 2015, 2021) suggested by the seismic reflection results (Supp. Fig. 2) is also revealed in our geo-electrical models (Fig. 7). It is noteworthy that the ‘upper lip’ of the ‘crocodile’ is represented by the LYD nappe (west part of the double thrust system) (Fig. 9b). In this structure, the main thrust fault and the Yangtze fault both connect a deep detachment layer (C2 beneath S2) in the middle crust, surrounding the major resistor (R2). The ‘upper lip’ (LYD nappe) can be attributed to the slipping of the upper crust and decoupling deformation between the upper and lower crust (Zhang et al., 2021) under compressional stress (Lü et al., 2015). The deformation is mainly developed in the LYD nappe system (upper crust), excluding the crustal basement (lower crust).

Furthermore, the geo-electrical models reveal two major interfaces in the upper-middle crust, with a northwestward dip of 20°–30° for the deeper interface (S2) and a 15°–25° dip for the shallower (SS1) (Fig. 7). The detachments (S2 and SS1) correspond to the unconformities of the Silurian and Triassic strata, as supported by structural geology research (e.g., Wang et al., 2012; Li et al., 2021 and references therein). The LYD, composed of well-developed thin-skinned tectonics, is hence characterized as a foreland thrust belt, caused by the collision between the Yangtze and North China.

However, a distinct nappe system is revealed in the JNO. The main thrust fault and several faults to the west of the Jiangnan fault connect with a deep conductive layer (C3 beneath S4) in the middle crust. This structural system and internally wrapped resistor (R3) constitute the JNO nappe (Fig. 9b). The JNO nappe strikes NE and dips SE. Its detached interfaces (S4 and SS2), which have a steep northwestward dip of 45°–60° in our models, can be attributed to the unconformities of the Cambrian and Neoproterozoic strata (Wang et al., 2012). In addition, the Precambrian basement is involved in the deformation of the JNO nappe, as evidenced by the structural geology and seismic reflection data (Wang et al., 2012; Lü et al., 2015). The thrusts revealed by vertically conductive belts overlying S4 (Fig. 7) hence may have extended into the crustal basement in the southeastern JNO. These steep and deep structures suggest a thick-skinned tectonics system, indicating a vertical uplift process.

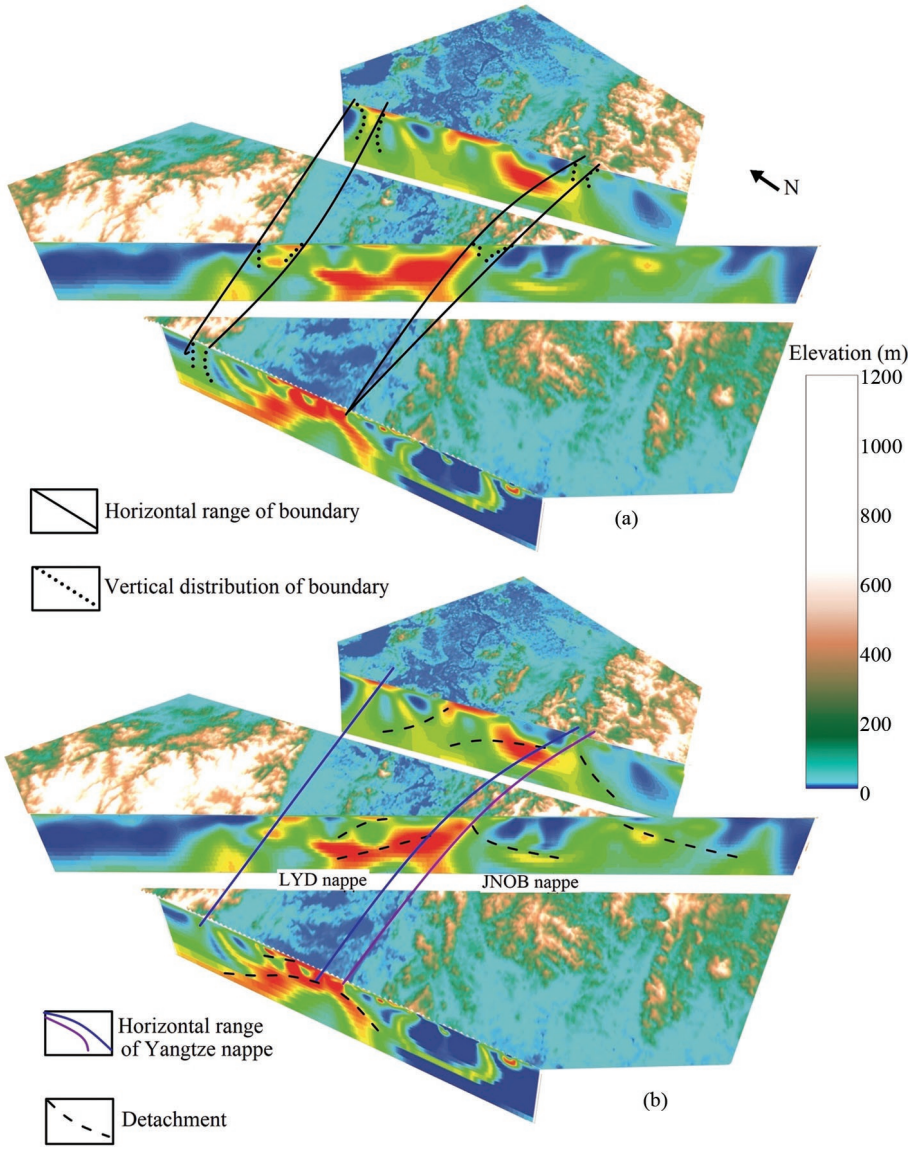

Fig. 9. Tectonic boundaries and nappe distribution.
(a) The boundaries' variation range in the crust; (b) the distribution of the LYD and JNO nappes.

It is noteworthy that the break-off point (beneath the WBJ) of the Yangtze subduction slab (Zhang et al., 2019a, 2020, 2021) beneath S3, could be a controlling factor that separates the two nappe units of the LYD and the JNO (Fig. 9b). Therefore, this thick-skinned tectonic system and the break-off of the subduction slab suggest a 'reworked' orogeny of the JNO, instead of a collisional orogeny.

5.2 Uplift evolution of the Jiangnan Orogen

In the JNO nappe, the newest involved strata were formed in the Middle Jurassic in a compressional setting (Lü et al., 2021), which were then covered by the volcanic rocks of the Late Jurassic–Early Cretaceous (Zhou et al., 2016; Liu et al., 2016). However, the process of eastward extrusion of the DOB from the Middle Triassic to the Early Jurassic (Li et al., 2010) resulted in the southeastward thrust nappe in the LYD (Dong et al., 2011). Therefore, the formation of the JNO nappe is probably later than that of the LYD. The fold type and thrust dipping in the JNO revealed in our models indicate a northwestward tectonic stress, which might result from the compression of the Paleo-Pacific Block in the Late Mesozoic (Song et al., 2012), rather than the E–W trend formed by the Triassic continent-continent collision with the North China craton (Li et al., 2011), as evidenced by the structural (crustal deformation), magmatic (granites) and geophysical (seismic reflection) study results (e.g., Lü et al., 2013, 2014, 2015; Shu et al., 2020 and references therein). Moreover, previous MT research (Zhang et al., 2019a, 2020) revealed the 'crocodile' structure and intra-continental subduction slab (Figs. 7), indicating an intacontinental subduction process after the collision between North China and Yangtze (Fig. 10a–b). As indicated by the large-scale mantle-derived magmatism (e.g., Zhou et al., 2016; Shu et al., 2020) and conductors in our geo-electrical models (C1 and eastern

C2), this intra-continental subduction slab of the Yangtze could have broken off from the Yangtze lithosphere (Zhang et al., 2019a, 2020; Fig. 10c) and led to the upwelling of the deep materials (Zhang et al., 2021; Li et al., 2021; Fig. 10d–e). A possible scenario for this to occur is the obstruction of the DOB and the northwestward compression of the Paleo-Pacific Block. The geochronological data (e.g., Zhou et al., 2009, 2016; Qi, 2019; Li et al., 2020 and references therein) show a regionally tectonic regime conversion time from ~145 Ma to ~135 Ma, as supported by the magmatic rocks with a distinct mixing level of the lower crust and the upper mantle. The later magma contains more mantle-derived materials, indicating a regime conversion from compression to extension.

Therefore, we propose a 'reworked' orogenic model to explain the formation of the JNO, consistent with the tectonic regime conversion. After the break-off of the intra-continental slab, hot material is suggested to have upwelled (Wang et al., 2004; Zhou et al., 2016) around the slab and led to the uplift of the JNO (Fig. 10c).

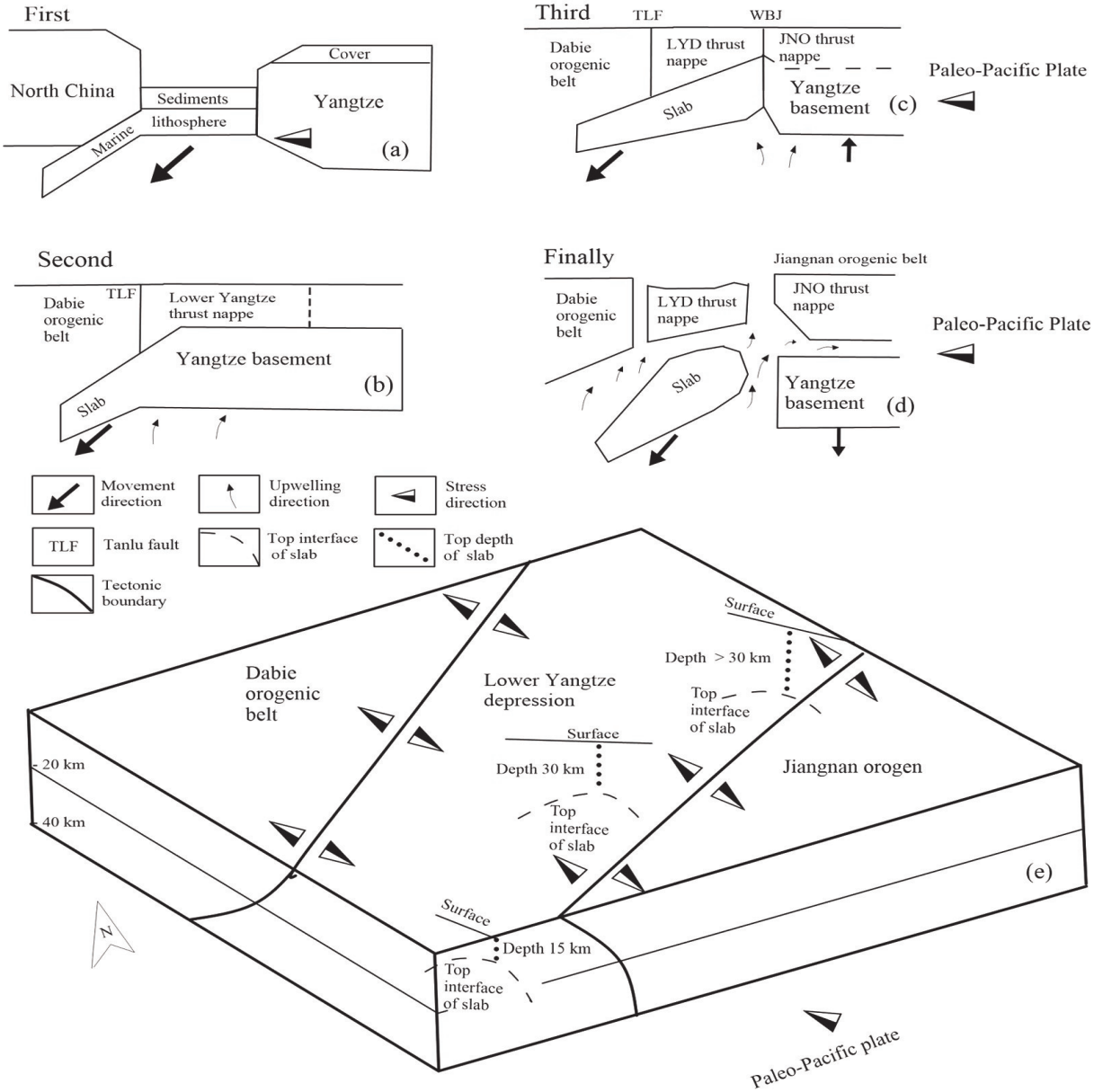

Fig. 10. Orogenic evolution during the Mesozoic.
(a) Yangtze moved towards the North China craton following the subduction (Zhang et al., 2019a); (b) decollement and thrust nappe structures were formed in the LYD during the collision process between North China and Yangtze; (c) uplift orogen and JNO nappe, which took the slab as the 'fulcrum', developed after the break-off of the subduction slab in the compression of the Paleo-Pacific Plate; (d) orogeny of the JNO was sustained by lithospheric delamination and crustal uplift induced by the slab break-off and compression on both sides of the JNO; (e) the extensional setting of the eastern Yangtze has formed since the Late Jurassic. TLF: Tancheng–Lujiang fault; LYD: Lower Yangtze Depression; JNO: Jiangnan Orogen; WBJ: western boundary of Jiangnan.

Furthermore, the fold basements, whose boundary is consistent with that between the LYD and the JNO in our geo-electrical models, do not support a subduction-collision process and a collisional orogeny beneath the JNO in the late Mesozoic. Therefore, we suggest that the 'reworked' orogeny of the JNO starts from an intra-continental uplift process that has occurred since the Middle Jurassic, considering its thick-skinned tectonics.

Moreover, the regional heat flow increases from ~50 mW/m^2 in the DOB to ~70 mW/m^2 in the JNO (Supp. Fig. 3), while the thickness of the 'thermal' lithosphere decreases from 140 to 60 km (He et al., 2001). It is widely accepted that the thermal contribution from the crust is greater than that from the mantle in the continental lithosphere (Lee, 1970). Therefore, the crust beneath the JNO can be inferred to release much more thermal energy than that beneath the DOB and LYD. Therefore, following the detachment of the Yangtze slab, the upwelling (C1 beneath S4) and spreading (C3 beneath S4) of the hot materials through the break-off point of the slab could have induced the decoupling of crust and upper mantle (Fig. 10d). The material flow could then have contributed to the continued intra-continental orogeny of the JNO (Fig. 10d–e), cooperating with the Paleo-Pacific plate, which provided the northwestward compressional setting. Overall, this uplift orogeny of the JNO contained two stages, including the firstly lithospheric uplift and then the secondly crustal uplift.

6 Conclusions

To better understand the evolution of the Jiangnan Orogen, high-quality magnetotelluric data were acquired and interpreted from the Dabie Orogenic Belt to the eastern Yangtze. Resistivity models are presented, revealing strong lateral variations in electrical structure in the mid-to-lower crust of the study area. A prominent NE–SW directed conductor is inferred as a large-scale detachment layer, which separates the resistive structures. On both sides of this major conductor, the southward extension of the Tancheng–Lujiang Fault is found in the Dabie Orogenic Belt and a new electrical boundary between the Jiangnan Orogen and the Lower Yangtze Depression is identified. This boundary controls the thrust nappe structures on both sides. In contrast to the Lower Yangtze Depression nappe developed in a collision process, the thick-skinned tectonic system of the Jiangnan Orogen nappe indicated by the geo-electrical structures suggests an orogeny independent of collision. We hence present a new 'intra-continental orogen' model to describe a 'reworked' orogenic process of the Jiangnan Orogen developed in the Late Mesozoic. Since the Middle Jurassic, the thrust-nappe develops in the Jiangnan Orogen, which is induced by an intra-continental uplift process caused by the material upwelling. This process is composed of at least two stages, from the lithosphere uplift to the crustal uplift.

It should be noted that the variation in the top depth of the slab indicates a vertical tearing between profile An and SP. However, our model cannot constrain structures in the gap between the profiles and east of 118.4°E. A carefully designed 3D MT array can test our hypothesis in our study region.

Acknowledgments

This study was funded by the Anhui Province Science Program (2018-g-1-4), the National Science Program (Nos. 41630320, 42174087) and the National Key R&D Program of China (No. 2016YFC0600201). The authors wish to thank Dr. Hao Dong (China's University of Geosciences, Beijing) for his help with this study.

Manuscript received Aug. 06, 2021
accepted Apr. 28, 2022
associate EIC: XIAO Wenjiao
edited by Jeffery J. LISTON and FEI Hongcai

Supplementary material to this article can be found online at https://doi.org/10.1111/1755-6724.14950.

References

Caldwell, T.G., Bibby, H.M., and Brown, C., 2004. The magnetotelluric phase tensor. Geophysical Journal International, 158(2): 457–469.

Chang, Y.F., Liu, X.P., and Wu, Y.C., 1991. The Copper-iron Belt of the Lower and Middle Reaches of the Changjiang River. Beijing: Geological Publishing House, 1–379 (in Chinese).

Chang, Y.F., Dong, S.W., and Hong, D.Z., 1996. On tectonics of "polybasement with one cover" in Middle–Lower Yangtze Craton, China. Volcanology & Mineral Resources, 17(S1): 1–15 (in Chinese with English abstract).

Charvet, J., Shu, L.S., Shi, Y.S., Guo, L.Z., and Faure, M., 1996. The building of South China: Collision of Yangtze and Cathaysia blocks, problems and tentative answers. Journal of Southeast Asian Earth Science, 13(3–5): 223–235.

Chen, J.F., Foland, K.A., Xing, F.M., Xu, X., and Zhou, T.X., 1991. Magmatism along the southeast margin of the Yangtze Block: Precambrian collision of the Yangtze and Cathaysia blocks of China. Geology, 19(8): 815–818.

Dong, S.W., Ma, L.C., Liu, G., Xue, H.M., Shi, W., and Li, J.H., 2011. On dynamics of the metallogenic belt of the Middle–Lower Reaches of the Yangtze River, eastern China. Acta Geologica Sinica, 85(5): 612–625 (in Chinese with English abstract).

Dong, H., Wei., W.B., Jin, S., Ye, G.F., Zhang, L.T., Jing, J.E., Yin, Y.T., Xie, C.L., and Jones, A., 2016. Extensional extrusion: Insights into south-eastward expansion of Tibetan Plateau from magnetotelluric array data. Earth and Planetary Science Letters, 454: 78–85.

Faure, M., Lin, W., and Breton, N.L., 2001. Where is the North China–South China block boundary in eastern China? Geology, 29(2): 119–122.

Ge, X., Shen, C.B., Yang, Z., Mei, L.F., Xu, S.H., Peng, L., and Liu, Z.Q., 2013. Low-temperature thermochronology Constraints on the Mesozoic–Cenozoic exhumation of the Huangling massif in the Middle Yangtze Block, Central China. Journal of Earth Science, 24(4): 541–552.

Guo, L.Z., Shi, Y.S., and Ma, R.S., 1977. On the research method and significance of the ancient trench island arc system. Geology of Fujian, 4: 1–24 (in Chinese).

He, L.J., Hu, S.B., and Wang, J.Y., 2001. The characteristics of the thermal structure of the lithosphere in East China. Progress in Natural Science, 11(9): 966–969 (in Chinese).

Hsü, K.J., Sun, S., Li, J.L., Chen, H.H., Pen, H.B., and Sengor, A.M.C., 1988. Mesozoic overthrust tectonics in South China. Geology, 16(5): 418–421.

Huang, J.Q., 1954. Main geological structural units in China. Beijing: Geological Publishing House, 1–150 (in Chinese).

Huang, J.Q., 1959. Some opinions on the compilation of the

Chinese geotectonic map. Geoscience Communication, 2: 3–8 (in Chinese).
Huang, J.Q., 1960. A preliminary summary of the basic characteristics of geological structure in China. Acta Geologica Sinica, 40(1): 1–31 (in Chinese).
Ichihara, H., and Mogi, T., 2009. A realistic 3-D resistivity model explaining anomalous large magnetotelluric phases: The l-shaped conductor model. Geophysical Journal International, 179(1): 14–17.
Jiang, G.M., Zhang, G.B., Lü, Q.T., Shi, D.N., and Xu, Y., 2013. 3-D velocity model beneath the Middle–Lower Yangtze River and its implication to the deep geodynamics. Tectonophysics, 606: 36–47.
Jones, A.G., 1992. Electrical properties of the continental lower crust. In: Fountain, D.M., Arculus, R.J., and Kay, R.W. (eds.), Continental Lower Crust. Elsevier, Amsterdam, 81–143.
Jones, A.G., 1983. On the equivalence of the "Niblett" and "Bostick" transformations in the magnetotelluric method. Journal of Geophysics, 53: 72–73.
Lee, W.H.K., 1970. On the global variations of terrestrial heat-flow. Physics of the Earth and Planetary Interiors, 2(5): 332–341.
Li, S.Z., Zhao, G.C., Zhang, G.W., Liu, X.C., Dong, S.W., Wang, Y.J., Liu, X., Suo, Y.H., Dai, L.M., Jin, C., Liu, L.P., Hao, Y., Liu, E.S., Wang, J., and Wang, T., 2010. Not all folds and thrusts in the Yangtze foreland thrust belt are related to the Dabie Orogen: Insights from Mesozoic deformation south of the Yangtze River. Geological Journal, 45(5–6): 650–663.
Li, S.Z., Zhang, G.W., Zhou, L.H., Zhao, G.C., Liu, X., Suo, Y.H., Liu, B., Jin, C., and Dai, L.M., 2011. The opposite Meso–Cenozoic intracontinental deformations under the super-convergence: Rifting and extension in the North China Craton and shortening and thrusting in the South China Craton. Earth Science Frontiers, 18(3): 79–107 (in Chinese with English abstract).
Li, S.Z., Zhao, G.C., Dai, L.M., Liu, X., Zhou, L.L., Santosh, M., and Suo, Y.H., 2012. Mesozoic basins in eastern China and their bearing on the deconstruction of the North China Craton. Journal of Asian Earth Sciences, 47: 64–79.
Li, X.Y., Zhu, P.M., Kusky, T.M., Gu, Y., Peng, S.B., Yuan, Y.F., and Fu, J.M., 2015. Has the Yangtze craton lost its root? A comparison between the North China and Yangtze cratons. Tectonophysics, 655: 1–14.
Li, Y., Yuan, F., Jowitt, S.M., Deng, Y.F., Hu, X.Y., Liu, G.X., Li, X.H., and Zhou, T.F., 2020. Geochronology, petrogenesis and metallogenic implications of mineralization-related intrusive rocks in the Xuancheng ore district, eastern China. Ore Geology Reviews, 135: 103690.
Li, C., Wang, Z., Lü, Q., Tan, Y., Li, L., and Tao, T., 2021. Mesozoic tectonic evolution of the eastern South China Block: A review on the synthesis of the regional deformation and magmatism. Ore Geology Reviews, 131: 104028.
Ling, M.X., Wang, F.Y., Ding, X., Hu, Y.H., Zhou, J.B., Zartman, R.E., Yang, X.Y., and Sun, W., 2009. Cretaceous ridge subduction along the lower Yangtze River belt, eastern China. Economic Geology, 104(2): 303–321.
Liu, L., Xu, X.S., and Xia, Y., 2016. Asynchronizing paleo-Pacific slab rollback beneath SE China: Insights from the episodic Late Mesozoic volcanism. Gondwana Research, 37: 397–407.
Lü, Q.T., Yan, J.Y., Shi, D.N., Dong, S.W., Tang, J.T., Wu, M.A., and Chang, Y.F., 2013. Reflection seismic imaging of the Lujiang–Zongyang volcanic basin, Yangtze Metallogenic Belt: An insight into the crust structure and geodynamics of an ore district. Tectonophysics, 606: 60–77.
Lü, Q.T., Dong, S.W., Shi, D.N., Tang, J.T., Jiang, G.M., and Zhang, Y.Q., 2014. Lithosphere architecture and geodynamic model of Middle and Lower Reaches of Yangtze Metallogenic Belt: A review from SinoProbe. Acta Petrologica Sinica, 30 (4): 889–906 (in Chinese with English abstract).
Lü, Q.T., Liu, Z.D., Dong, S.W., Yan, J.Y., and Zhang, Y.Q., 2015. The nature of Yangtze River deep fault zone: Evidence for deep seismic data. Chinese Journal of Geophysics, 58(12): 4344–4359 (in Chinese with English abstract).
Lü, Q.T., Meng, G.X., Zhang, K., Liu, Z.D., Yan, J.Y., Shi, D.N., Han, J.G., and Gong, X.J., 2021. The lithospheric architecture of the Lower Yangtze Metallogenic Belt, East China: Insights into an extensive Fe-Cu mineral system. Ore Geology Reviews, 132: 103989.
Mao, J.R., Li, Z.L., and Ye, H.M., 2014. Mesozoic tectono-magmatic activities in South China: Retrospect and prospect. Science China: Earth Sciences, 57(12): 2853–2877.
Newman, G.A., and Alumbaugh, D.L., 2000.Three-dimensional magnetotellutric inversion using non-linear conjugate gradients. Geophysical Journal International, 140: 410–424.
Ni, J.L., Liu, J.L., Tang, X.L., Yang, H.B., Xia, Z.M., and Guo, Q.J., 2013. The Wulian metamorphic core complex: A newly discovered metamorphic core complex along the Sulu orogenic belt, eastern China. Journal of Earth Science, 24(3): 297–313.
Pirajno, F., 2013. The Geology and Tectonic Settings of China's Mineral Deposits. Springer, New York.
Qi, H.S., 2019. Comparing geochemistry study of porphyry copper-gold deposits in different tectonic environments: A case study of Grasberg, Papua, Indonesia and Chating, Anhui Province. Hefei: University of Science and Technology of China (in Chinese with English abstract).
Ren, J.S., Niu, B.G., He, Z., Xie, G., and Liu, Z.G., 1997. Tectonic frame and geodynamic evolution of eastern China. Geological Research, 29(30): 43–55 (in Chinese with English abstract).
Rodi, W.L., Mackie, R.L., 2001. Nonlinear conjugate gradients algorithm for 2-D magnetotelluric inversion. Geophysics, 61 (1): 174–187.
Shu, L.S., Shi, Y.S., Guo, L.Z., Charvet, J., and Sun, Y., 1995. Plate terrane structure and collisional orogeny in the middle part of Jiangnan. Nanjing: Nanjing University Press, 1–170 (in Chinese).
Shu, L.S., Faure, M., Yu, J.H., and Jahn, B.M., 2011. Geochronological and geochemical features of the Cathaysia block (South China): New evidence for the Neoproterozoic breakup of Rodinia. Precambrian Research, 187(3–4): 263–276.
Shu, L.S., Chen, X.Y., and Lou, F.S., 2020. Pre-Jurassic tectonics of South China. Acta Geologica Sinica, 94(2): 333–360 (in Chinese with English abstract).
Song, C.Z., Jiang, Q.S., Li, J.H., Yan, J., Shi, Y.H., Han, C.S., Huang, W.P., and Yu, G., 2012. Relationship between structures and their controls to ores in the southern margin of Fanchang Basin in Anhui Province. Acta Petrologica Sinica, 28(10): 3197–3208 (in Chinese with English abstract).
Wang, P.C., Li, S.Z., Liu, X., Yu, S., Liu, B., Suo, Y.H., Xue, Y.C., and An, H.T., 2012. Yanshanian fold-thrust tectonics and dynamics in the Middle–Lower Yangtze River area, China. Acta Petrologica Sinica, 28(10): 3418–3430 (in Chinese with English abstract).
Wang, Q., Zhao, Z.H., Xiong, X.L., and Xu, J.F., 2001. Melting of the underplating basaltic lower crust: Evidence from the Shaxi adakite-like sodium-rich quartz diorite–porphyrite in Anhui Province. Geochimica, 30(4): 353–362 (in Chinese with English abstract).
Wang, X.L., Zhou, J.C., Qiu, J.S., and Gao, J.F., 2004. Geochemistry of the Meso- to Neo-proterozoic basic-acid rocks from Hunan Province, South China: Implications for the evolution of the western Jiangnan orogen. Precambrian Research, 135: 79–103.
Wang, X.L., Zhou, J.C., Chen, X., Zhang, F.F., and Sun, Z.M., 2017. Formation and evolution of the Jiangnan Orogen. Bulletin of Mineralogy, Petrology and Geochemistry, 36(5): 714–735 (in Chinese with English abstract).
Wang, Y.J., Zhang, F.F., Fan, W.M., Zhang, G.W., Chen, S.Y., Cawood, P.A., and Zhang, A.M., 2010. Tectonic setting of the South China Block in the early Paleozoic: Resolving intra-continental and ocean closure models from detrital zircon U-Pb geochronology. Tectonics, 29(6): TC6020.
Wong, J., Sun, M., Xing, G.F., Li, X.H., Zhao, G.C., Wong, K., and Wu, F.Y., 2011. Zircon U-Pb and Hf isotopic study of Mesozoic felsic rocks from eastern Zhejiang, South China: Geochemical contrast between the Yangtze and Cathaysia

blocks. Gondwana Research, 19(1): 244–259.
Xu, J.H., Sun, S., and Li, J.L., 1987. South China Orogen but not the South China platform. Science in China Series B-Chemistry, Life Sciences & Earth Sciences, 17(10): 1107–1115.
Xu, B., Guo, L.Z., and Shi, Y.S., 1992. Proterozoic terrane and polyphase collision in Anhui Zhejiang Jiangxi area Mountain belt. Beijing: Geological Publishing House, 1–120.
Zhai, M.G., and Zhou, Y.Y., 2015. General Precambrian geology in China. In: Zhai, M.G. (ed.), Precambrian Geology of China, Springer Geology, 3–58.
Zhang, K., Wei, W.B., Lü, Q.T., and Jin, S., 2011. The study of 2 -D nonlinear conjugate gradients inversion of borehole to surface magnetotelluric. Acta Geologica Sinica, 85(5): 915–924 (in Chinese with English abstract).
Zhang, K., Dong, H., Yan, J.Y., Lu, Q.T., Wei, W.B., and He, Y.X., 2013. A NLCG inversion method of magnetotellurics with parallel structure. Chinese Journal of Geophysics, 56 (11): 3922–3931 (English edition).
Zhang, K., Wei, W.B., and Lü, Q.T., 2014a. Four changes for efficiency and practicality on previous 3D MT NLCG inversion algorithm. Acta Geodaetica et Geophysica, 49(4): 551–563.
Zhang, K., Wei, W.B., Lü, Q.T., Dong, H., and Li, Y.Q., 2014b. Theoretical assessment of 3-D magnetotelluric method for oil and gas exploration: Synthetic examples. Journal of Applied Geophysics, 106: 23–36.
Zhang, K., Yan, J.Y., Lü, Q.T., Wei, W.B., Wang, H.F., and Zhang, Y.W., 2016. Correction of magnetotelluric static shift by analysis of 3D forward modeling and measured test data. Exploration Geophysics, 47(2): 100–107.
Zhang, K., Yan, J.Y., Lü, Q.T., Zhao, J.H., and Hu, H., 2017. Three-dimensional nonlinear conjugate gradient parallel inversion with full information of marine magnetotellurics. Journal of Applied Geophysics, 139: 144–157.
Zhang, K., Lü, Q.T., Yan, J.Y., Shao, L.S., Guo, D., and Zhang, Y.W., 2019a. The subduction and continental collision of the North China and Yangtze blocks: Magnetotelluric evidence from the Susong–Anqing section of Western Anhui, China. Geophysical Journal International, 216(3): 2114–2128.
Zhang, K., Lü, Q.T., Yan, J.Y., Hu, H., Fu, G.M., and Luo, F., 2019b. The three-dimensional electrical structure and metallogenic prospect of the Ning (Nanjing)–Wu (Wuhu) basin and the southern adjacent area in eastern China. Journal of Asian Earth Sciences, 173(1): 304–313.
Zhang, K., Lü, Q.T., Zhao, J.H., Yan, J.Y., Hu, H., Luo, F., Fu, G.M., and Tan, X., 2020. Magnetotelluric evidence for the multi-microcontinental composition of eastern South China and its tectonic evolution. Scientific Reports, 10: 13105.
Zhang, K., Lü, Q.T., Lan, X.Y., Guo, D., Wang, Q.N., Yan, J.Y., and Zhao, J.H., 2021. Magnetotelluric evidence for crustal decoupling: Insights into tectonic controls on the magmatic mineral system in the Nanling–Xuancheng area, SE China. Ore Geology Reviews, 131: 104045.
Zhang, Y.Q., and Dong, S.W., 2019. East Asia multi-plate convergence in the late Mesozoic and the development of continental tectonic systems. Journal of Geomechanics, 25(5): 613–641 (in Chinese with English abstract).
Zhao, G.C., 2015. Jiangnan Orogen in South China: Developing from divergent double subduction. Gondwana Research, 27: 1173–1180.
Zhao, T., Zhu, G., Lin, S.Z., and Wang, H.Q., 2016. Indentation-induced tearing of a subducting continent: Evidence from the Tan-Lu Fault Zone, East China. Earth-Science Reviews, 152: 14–36.
Zheng, Y.F., Chen, R.X., Xu, Z., and Zhang, S.B., 2016. The transport of water in subduction zones. Science China Earth Sciences, 59(4): 651–681.
Zhou, J.C., Wang, X.L., and Qiu, J.S., 2009. Geochronology of Neoproterozoic mafic rocks and sandstones from northeastern Guizhou, South China: Coeval arc magmatism and sedimentation. Precambrian Research, 170(2): 27–42.
Zhou, T.F., Wang, S.W., Yuan, F., Fan, Y., Zhang, D.Y., Chang, Y.F., and White, N.C., 2016. Magmatism and related mineralization of the intra-continental porphyry deposits in the Middle–Lower Yangtze River Valley Metallogenic Belt. Acta Petrologica Sinica, 32(2): 271–288 (in Chinese with English abstract).

About the first author

ZHANG Kun, male, born in 1983 in Tianjin; Ph.D.; graduated from China's University of Geosciences (Beijing); research fellow at the Chinese Academy of Geological Sciences. He is currently interested in the study of deep earth exploration and magnetotelluric techniques. E-mail: zhangkun1010@163.com.

About the corresponding author

LÜ Qingtian, male, born in 1964 in Nanyang, Henan Province; Ph.D.; graduated from the Changchun Institute of Geology; research fellow of the Chinese Academy of Geological Sciences. He is currently interested in the study of deep earth exploration and mineral systems. E-mail: lqt@cags.ac.cn.